# Fano resonances in quantum transport with vibrations

Ajith Ramachandran,[1] Michael Genkin,[2] Auditya Sharma,[1] Alexander Eisfeld,[2]
Sebastian Wüster,[1,*] and Jan-Michael Rost[2]

[1]*Department of Physics, Indian Institute of Science Education and Research, Bhopal, Madhya Pradesh 462 066, India*
[2]*Max Planck Institute for the Physics of Complex Systems, Nöthnitzer Straße 38, D-01187 Dresden, Germany*

Quantum-mechanical scattering involving continuum states coupled to a scatterer with a discrete spectrum gives rise to Fano resonances. Here we consider scatterers that possess internal vibrational degrees of freedom in addition to discrete states. Entanglement between the scattered excitation and vibrational modes complicates analytical and numerical calculations considerably. For the example of one-dimensional scattering we develop a multichannel quantum scattering approach which can determine reflection and transmission probabilities in the presence of vibrations. Application to a linear chain coupled to a control unit containing vibrating sites shows that vibrational degrees of freedom can have a profound effect on quantum transport. For suitable parameters, spectral regions which are opaque in the static case can be rendered transparent when vibrations are included. The formalism is general enough to be applicable to a variety of platforms for quantum transport including molecular aggregates, cold atom chains, quantum-dot arrays and molecular wires based on conjugated polymers.

## I. INTRODUCTION

Quantum transport of excitation, energy, and entanglement are fundamental features of a wide range of systems ranging from quantum aggregates of organic molecules [1–3], photosynthetic complexes [4–6], and cold atoms [7–11] to quantum-dot assemblies [12]. Such transport systems usually involve a regular part enabling wavelike transport with continuous wave numbers and may contain a second part consisting of small subunits with a discrete spectrum which couple to the regular part and affect the transport. Generically, this scenario gives rise to Fano resonances, "bound states in the continuum" originally described as "strange discrete eigenvalues" by von Neumann and Wigner in 1929 [13]. They cause characteristic asymmetric features in the transport spectrum [14–16], also known as Fano profiles. The resonances even lead to complete reflection or complete transmission at certain resonant energies, a useful resource for control and switching applications [17–20].

Apart from Fano resonances, transport is often affected by internal vibrations or phonons, e.g., electron-phonon coupling in long conjugated molecules [21,22] or molecular aggregates [23]. Although mostly seen as impeding transport but inevitable, in Rydberg aggregates atomic motion can also induce quantum transport [10,24–26]. Here, we demonstrate how atomic motion can serve to create a switch in transport systems. More specifically, we investigate quantum transport along the regular part of the system beyond a localized "obstacle," a subunit with one dominant vibrational degree of freedom. We will see that the transported excitations become entangled with vibrations and that the reflection and

transmission profiles based on Fano resonances are qualitatively altered if the subunit can be vibrationally excited compared to a transport system with a *static* subunit. Thereby, Fano resonances can be put to work for sensing and switching in transport transport systems even in the presence of directed or thermal motion. However, incorporating electron-vibrational coupling into quantum transport studies is a challenging problem. It has been tackled using perturbative approaches for wires on the molecular or atomic scale [27,28], scattering theory [29,30], Green's function methods [31–34], master and quantum kinetic equations [35], reduced electron-density matrix approaches [36], or a semiclassical treatment of the motion and approaches based on nonequilibrium statistical physics [37].

In the following, we formulate an alternative approach, which can exactly treat quantum transport and a few vibrations in a multichannel quantum scattering framework. We apply our theory to quantum transport on a long one-dimensional chain or wire coupled to a control unit (CU) that gives rise to Fano resonances in the transmission spectrum which is strongly modified by active vibrational modes of the CU. To be specific we will cast our results in terms of a chain consisting of atoms or molecules. However, the results more generally apply to discrete chains, such as conjugated polymers [38,39] in the tight-binding approximation, molecular wires [40,41], and coupled quantum dots [42–44] with involvement of phonons or optomechanical arrays [45,46]. To stress the applicability of the method in different contexts, we refrain from making reference to a specific platform. However, exemplary realizations are provided in Appendix F. Reference to a "monomer" in the subsequent text, thus, refers to any single site of the aforementioned transport systems.

Our article is organized as follows. To render our approach better comprehensible we first formalize our exemplary
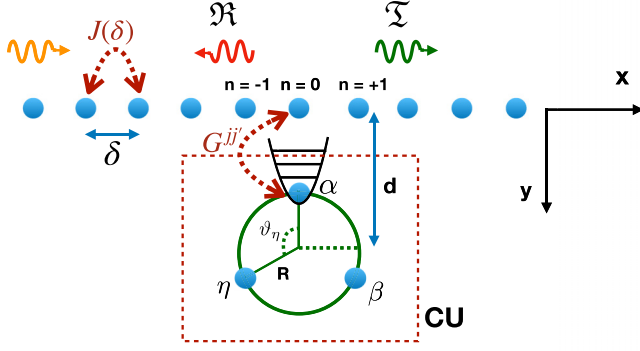
*sebastian@iiserb.ac.in

FIG. 1. Sketch of the Fano-Anderson chain with vibrating elements. $N$ static monomers are arranged in an equidistant linear chain and three monomers $\alpha$, $\beta$, $\eta$ are arranged within a control unit CU confined to a ring of radius $R$. The center of the ring is at a distance $d$ from the chain. The angular coordinates of the monomers on the ring are $\vartheta_j$ with $\vartheta_j = 0$ corresponding to the north pole. Two monomers are fixed at angles $\vartheta_\eta$ and $\vartheta_\beta$, whereas the third one (angle $\vartheta_\alpha$) is mobile within a harmonic trap. A wave packet carrying a single electronic excitation approaching the Fano defect from the far left (yellow) may be reflected (red) or transmitted (green) by the latter.

transport system in Sec. II including a comprehensive description of the Fano-Anderson chain in Sec. II A and entanglement in Sec. II B. The multichannel quantum scattering method is introduced in Sec. III. In Sec. IV we apply the method to investigate excitation transport in the absence (Sec. IV A) and presence (Sec. IV B) of vibrational motion. The results are summarized in Sec. V.

## II. MODEL AND METHODS

### A. Fano-Anderson chain with vibrating elements

We consider a linear chain of $N$ monomers, which is in contact with a control unit containing three monomers confined on a circle of radius $R$ as sketched in Fig. 1. Although many CUs are conceivable, our CU is small, convenient to design as we will discuss later, and most importantly, vibrations of our control unit can affect transport *significantly*. We refer to the electronic state of the system with a single excitation on monomer or site $n$ as $|\pi_n\rangle$. For atomic or molecular systems this implies that only the $n$th entity is excited with all others in the ground state. For other transport systems mentioned in the Introduction, the state would imply a nearly empty lattice of sites with a single particle filling the $n$th site. From here on we consider the total number of monomers on the chain $N$ to be even with the monomer $n = 0$ situated in the middle of the chain. The index $n$ fulfills $n \in \mathbb{Z}_N \cup \{\alpha, \beta, \eta\}$ with $\mathbb{Z}_N = \{-N/2, \ldots, 0, \ldots, N/2 - 1\}$ with integer $n \in \mathbb{Z}_N$ indicating an excitation on the main chain and $n \in \{\alpha, \beta, \eta\}$ on the CU, see Fig. 1.

Interaction between sites enables the excitation (e.g., excited state or electron) to move along the chain, whereas conserving their total number where we consider a single excitation only. For simplicity, we restrict ourselves to nearest-neighbor interactions of strength $J$ in the

chain Hamiltonian,

$$\hat{H}_C = J \sum_{n \in \mathbb{Z}_N} (|\pi_n\rangle \langle \pi_{n+1}| + |\pi_{n+1}\rangle \langle \pi_n|). \quad (1)$$

In addition to the electronic degrees of freedom discussed so far, we have to formalize the vibrational degree of freedom in the CU which can couple to the electron dynamics. To this end we consider the angular coordinate $\vartheta_n$ of the control unit monomers $n \in \{\alpha, \beta, \eta\}$ to change according to the harmonic-oscillator Hamiltonian,

$$\hat{H}_{\text{vib}} = - \sum_{n \in \{\alpha, \beta, \eta\}} \frac{\hbar^2}{2I_n} \nabla_{\vartheta_n}^2 + \hat{V}(\boldsymbol{\vartheta}), \quad (2a)$$

$$\hat{V}(\boldsymbol{\vartheta}) = \sum_{n \in \{\alpha, \beta, \eta\}} \frac{1}{2} M_n \omega_n^2 R^2 \left\{ 2\left[1 - \cos\left(\vartheta_n^{(0)} - \vartheta_n\right)\right]\right\}$$

$$\approx \sum_{n \in \{\alpha, \beta, \eta\}} \frac{1}{2} M_n \omega_n^2 R^2 \left(\vartheta_n^{(0)} - \vartheta_n\right)^2, \quad (2b)$$

with the equilibrium positions $\vartheta_n^{(0)}$ and the moment of inertia $I_n = M_n R^2$, whereas $M_n$ is the effective mass of monomer $n$ and $\boldsymbol{\vartheta} = [\vartheta_\alpha, \vartheta_\beta, \vartheta_\gamma]^T$ is the vector of all angles.

For simplicity, we consider the two monomers $\beta$ and $\eta$ so tightly confined in their respective harmonic potential with $\hbar\omega_\beta = \hbar\omega_\eta \gg J$ that there is a negligible extension of their ground-state wave function. They then remain in the ground state for all energies considered, and we can neglect their vibrational degrees of freedom. Only monomer $\alpha$ has a harmonic confinement $\hbar\omega_\alpha \ll J$ such that several vibrational states $|j\rangle$ contribute. From here on, we, thus, define $\omega \equiv \omega_\alpha$ to simplify the notation. In that case, the Hamiltonian $\hat{H}'_{\text{vib}}$ possesses a discrete energy spectrum given by $\hat{H}'_{\text{vib}} |\Phi_j\rangle = \mathcal{E}_j |\Phi_j\rangle = \hbar\omega(j + \frac{1}{2}) |\Phi_j\rangle$. The complete orthonormal basis set of the total Hilbert space is formed by the direct products $|nj\rangle = |\pi_n\rangle_{el} \otimes |\Phi_j\rangle_{\text{vib}}$, $n \in \mathbb{Z} \cup \{\alpha, \beta, \eta\}$. In the joint Hilbert space, the total Hamiltonian of the system is given by

$$\hat{H} = \hat{H}_C \otimes \mathbb{1}_{\text{vib}} + \hat{H}_U + \hat{H}_{UC} + \hat{H}_{\text{vib}}, \quad (3a)$$

where $\mathbb{1}_{\text{vib}}$ is the identity in the vibrational space and the vibrational motion affects the dynamics in the CU, described by $H_U$ and $H_{\text{vib}}$, and couples to the chain according to $H_{UC}$,

$$\hat{H}_U = \sum_{n,n' \in \{\alpha, \beta, \eta\}} \sum_{jj'} F_{nn'}^{jj'} |nj\rangle \langle n'j'|, \quad (3b)$$

$$\hat{H}_{UC} = \sum_{jj'} G^{jj'} (|0j\rangle \langle \alpha j'| + |\alpha j'\rangle \langle 0j|), \quad (3c)$$

$$\hat{H}_{\text{vib}} = \sum_{nj} \mathcal{E}_j |nj\rangle \langle nj| = \mathbb{1}_{el} \otimes \sum_j \mathcal{E}_j |j\rangle \langle j|. \quad (3d)$$

where $\mathbb{1}_{el}$ is the electronic identity. The coupling matrix elements are

$$F_{nn'}^{jj'} = \int d\boldsymbol{\vartheta} \, \Phi_j^*(\boldsymbol{\vartheta}) F_{nn'}(\boldsymbol{\vartheta}) \Phi_{j'}(\boldsymbol{\vartheta}), \quad (3e)$$

$$G^{jj'} = \int d\boldsymbol{\vartheta} \, \Phi_j^*(\boldsymbol{\vartheta}) G(\boldsymbol{\vartheta}) \Phi_{j'}(\boldsymbol{\vartheta}), \quad (3f)$$

where $F_{nn'}(\boldsymbol{\vartheta})$ and $G(\boldsymbol{\vartheta})$ are $\boldsymbol{\vartheta}$-dependent hopping parameters. To keep our approach general enough to apply to diverse

transport systems as discussed in the Introduction, the basic formalism does not make reference to a specific model of interactions, except that $\hat{H}_U$ and $\hat{H}_{UC}$ should depend on the spatial coordinates $\vartheta$ of the control unit monomers. They, therefore, also depend on the two parameters $d$ and $R$ of the design, the distance from the center of the control unit to the main chain, and the radius of the CU, respectively (see Fig. 1 for the geometry). Note that through the dependence of the dynamics on $\vartheta$, the vibrational motion of the monomer in the ring will be coupled to the excitation transport on the chain. For the presented numerical results, we use dipole-dipole interactions for which the hopping parameters scale with the inverse cubed distance between the sites, for details see Appendix B.

In molecular physics, corrections beyond the harmonic approximation are frequently required to describe the vibrational degrees of freedom. Since our approach is based on a matrix formulation, it can adopt this generalization easily. Only the vibrational spectrum of $H'_{\text{vib}}$ and the value of the overlap integrals in Eqs. (3e) and (3f) would change.

We are interested in the quantum transport of an excitation passing the control unit on the chain from the left to the right. In the absence of the control unit the transport can be described in terms of the eigenstates of (1). They form an exciton band of energies $E_k = 2J \cos k$ with $|E_k| \leqslant 2J$, where $k$ is the wave vector of the incoming excitation [47]. We refer to this band as continuous in the following, implying the limit of infinitely many monomers in the chain, whereas for numerical calculations we employ, of course, a finite number of elements on the chain $N = 1000$. Subject to dispersion, the excitation can migrate across the chain. To enable the CU to act as a scatterer and, therefore, to efficiently influence the transport, $J$ will be chosen on the order of all other energy scales in the system.

This influence is mediated through the interactions between the continuous band of the linear chain and the three discrete eigenstates of the scatterer belonging to the CU and leads to modifications of the transmission characteristics by virtue of the Fano resonance [19,48,49]. In the case of static interactions, i.e., without vibrations in $\vartheta$, it is well understood how the control unit affects transport on the chain [14,16,19]. Specifically, for incoming wave energies that match an eigenenergy of the isolated static CU, transmission will be fully suppressed as discussed later. The width of such a resonance dip in the transmission profile depends on the strength of the interaction $G$ between the main chain and the control unit in (3c).

### B. Quantum dynamics and entanglement

We now explore the fate of an initial single excitation prepared on the far left side of the linear chain of monomers on its path across the chain. It must eventually impact the scattering region of the CU. In a time-dependent picture, we start from an initial state of the form

$$|\Psi(t = 0)\rangle = |\psi_{\text{ini}}\rangle \otimes |j_{\text{in}}\rangle , \qquad (4)$$

where $|j_{\text{in}}\rangle$ is the initial vibrational state, chosen as eigenstate of the vibrational Hamiltonian, and $|\psi_{\text{ini}}\rangle$ is the electronic excited state. We take it to be localized near a site $n_0 < 0$ with
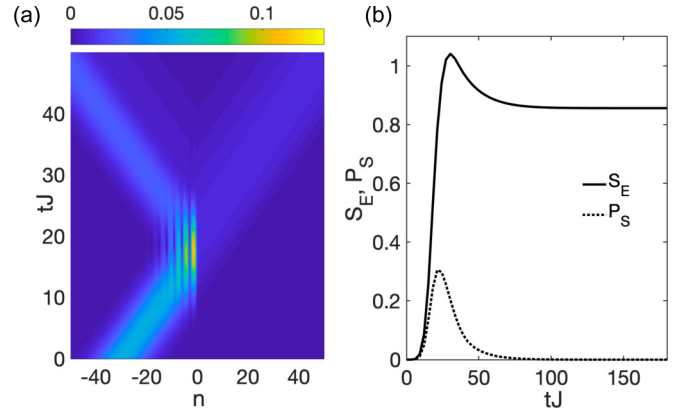


FIG. 2. (a) Evolution of the excitation probability $p_n = \sum_j |\psi_{nj}(t)|^2$ on the main chain, allowing vibrations of site $\alpha$. Populations on the CU are not shown. The vibration frequency is $\hbar\omega = 0.01J$, and other parameters are given in Ref. [50] for a chain with 1000 monomers. An excitation initially localized near $n = -30$ moves towards the right with energy $E = 1J$ and reflects back from the scattering region. The $x$ axis indicates the position on the chain in terms of monomer indices $n$. (b) The von Neumann entropy $S_E$ (6) as a function of time. The total excitation probability $P_U = \sum_{n \in \{\alpha,\beta,\eta\}j} |\psi_{nj}(t)|^2$ on the scattering control unit CU is also shown.

negligible amplitude on sites $n \geqslant 0$. Specifically we choose $\langle n|\psi_{\text{ini}}\rangle = \mathcal{N} \exp[-(n-n_0)^2/\sigma^2 + ik_{\text{in}}n]$, where $\mathcal{N}$ is a normalization factor and $k_{\text{in}}$ the central incoming wave number. The subsequent quantum dynamics of this wave packet is governed by the time-dependent Schrödinger equation (TDSE) $i\hbar \, d\Psi/dt = \hat{H}\Psi$ with $\hat{H}$ from (3a). The state can be expanded as

$$|\Psi(t)\rangle = \sum_{nj} \psi_{nj}(t) |nj\rangle . \qquad (5)$$

An example of such a scattering process is shown in Fig. 2(a) where the time dependence of the population on the sites $n$ of the chain is displayed. Populations of CU monomers are not shown. One sees that the incoming wave packet moves with constant velocity. Close to the time $t_c$ when the center of the wave packet reaches the site $n = 0$, the scattering site which is closest to the CU, an interference pattern appears. After the collision for $t > t_c$, one can clearly see the transmitted and reflected wave packet.

For times $t < t_c$, before the excitation reaches the CU, the vibrational degrees of freedom of the CU remain in their initial state $|j_{\text{in}}\rangle$ and the dynamics of the system is exclusively governed by $\hat{H}_C$. As the excitation hits the scattering region, the other terms in the Hamiltonian become important and vibronic quantum dynamics ensues for a finite time interval, until the excitation completely leaves the scattering region. The postcollision dynamics is again governed by $\hat{H}_C$. The final outcome of the scattering event is the splitting of the excitation probability into transmitted (right moving) and reflected (left moving) parts and a possible change of the internal vibrational state of the scatterer into some general superposition of vibrational eigenstates. Each vibrational state contributes to the outcome of the scattering process leaving multiple outgoing channels for the scattering.

An immediate consequence of the dependence of the scattering outcome on vibrational states of the CU is the creation of entanglement between the electronic and vibrational states during the scattering process. Entanglement can be quantified by the von Neumann entropy,

$$S_E = -\text{tr}(\rho_{\text{el}} \ln \rho_{\text{el}}), \tag{6}$$

where tr denotes the trace and $\rho_{\text{el}}$ the reduced electronic density matrix obtained by tracing out the vibrational degrees of freedom of the system [51], i.e., $\rho_{\text{el}} = \sum_j \langle j | \hat{\rho} | j \rangle$ with $\hat{\rho} = |\Psi(t)\rangle \langle \Psi(t)|$ and $|\Psi(t)\rangle$ in Eq. (5). This entropy is zero if the electronic and vibrational degrees of freedom are separable and equal to $\ln D$ for a maximally entangled state, if the reduced Hilbert space is $D$ dimensional. We see in Fig. 2(b) that before the wave packet hits the scattering region, the electronic and vibrational states are not entangled and the entropy is zero. As expected the entropy increases close to the impact time $t_c$, indicating the development of entanglement between electronic and vibrational states. This entanglement persists for long times, even after the excitation on the CU [dashed line in Fig. 2(b)] has dropped to zero again.

Conceptually, this means that even at a time $t = 100/J$ when the exciton wave packet has mostly returned to the main chain it remains intricately linked with the scatterer through entanglement with vibrational states. The entanglement leads to practical difficulties using conventional approaches, such as the transfer matrix method (TMM). The electronic and vibrational parts cannot be treated separately. Transmission, however, depends on the vibrational state giving rise to multiple channels. The incorporation of those channels for scattering leads to a cumbersome set of nonlinear equations in the TMM.

Therefore, we develop in the following a multichannel quantum scattering method (QSM) that can handle the entanglement discussed above as well as the effect of internal vibrations of the CU on quantum transport through the chain.

## III. MULTICHANNEL QUANTUM SCATTERING METHOD

Although we will use solutions of the TDSE for verification, we switch now to a time-independent framework in which scattering processes are usually more easily understood based on stationary scattering states. Consequently, we seek a solution of the eigenvalue problem,

$$\hat{H} |\Psi\rangle = E |\Psi\rangle, \tag{7}$$

with

$$|\Psi\rangle = \sum_{nj} \psi_{nj} |nj\rangle, \tag{8}$$

in analogy to the expansion of the time-dependent state (5). We intend to solve (7) for the case of an exciton wave coming in from the left with momentum $k_{\text{in}} > 0$ and the CU in the specific state $|j_{\text{in}}\rangle$ with vibrational quantum number $j_{\text{in}}$. (More complex initial vibrational states could be generated from these solutions by superposition.) The desired eigenstate $|\Psi\rangle$ is subject to the boundary conditions,

$$\psi_{nj} = \delta_{jj_{\text{in}}} e^{+ik_{\text{in}}n} + \Re_j(k_{\text{in}}) e^{-ik_j n}, \qquad n < 0 \tag{9}$$

for $n$ on the left side of the chain and analogously for $n$ on the right side of the chain,

$$\psi_{nj} = \mathfrak{T}_j(k_{\text{in}}) e^{+ik_j n}, \qquad n > 0. \tag{10}$$

Here, $\Re_j(k_{\text{in}})$ and $\mathfrak{T}_j(k_{\text{in}})$ are complex reflection and transmission amplitudes containing all information about the scattering outcome, and the momentum $k_j > 0$ of the $j$th channel is fixed by energy conservation $E = \mathcal{E}_{j_{\text{in}}} + E_{k_{\text{in}}} = \mathcal{E}_j + E_{k_j}$ for the exciton band energies $E_k$ and the vibrational energies $\mathcal{E}_j$ as defined earlier. The probability of transmission $T_j(k_{\text{in}})$ is given by the ratio between the transmitted and incoming flux in channel $j$,

$$T_j(k_{\text{in}}) = |\mathfrak{T}_j(k_{\text{in}})| \frac{\sin k_j}{\sin k_{\text{in}}}. \tag{11}$$

Similarly, the reflection coefficient $R_j(k_{\text{in}})$ is given by the ratio between reflected and incoming flux in channel $j$,

$$R_j(k_{\text{in}}) = |\Re_j(k_{\text{in}})| \frac{\sin k_j}{\sin k_{\text{in}}}. \tag{12}$$

Conservation of probability implies

$$\sum_j [T_j(k_{\text{in}}) + R_j(k_{\text{in}})] = 1, \tag{13}$$

and can serve as a consistency check of the final results.

In order to construct the desired stationary scattering state $|\Psi\rangle$, one needs to substitute the boundary conditions (9) and (10) back into the time-independent Schrödinger equation (7) and solve for $\Re_j$ and $\mathfrak{T}_j$. Exciton-phonon coupling links all vibrational components of the wave function, rendering the equation hard to solve for many vibrational levels of the scatterer.

Instead of tackling this problem directly, we employ a well-established trick [52,53] based on backward propagation. We convert the original Eq. (7) into a collection of auxiliary eigenproblems,

$$\hat{H} |\Psi^{(j_0)}\rangle = E |\Psi^{(j_0)}\rangle, \tag{14}$$

subject to new boundary conditions,

$$\psi_{nj}^{(j_0)} = A_j^{j_0} e^{+ik_j n} + (\delta_{jj_0} - A_j^{j_0}) e^{-ik_j n} \quad (n \leqslant 0) \tag{15}$$

$$\psi_{nj}^{(j_0)} = \delta_{jj_0} e^{+ik_{j_0}n} \quad (n \geqslant 0). \tag{16}$$

Here, the vibrational index $j_0$ is fixed but arbitrary, not related to $j_{\text{in}}$. We, thus, specify the vibrational quantum number for the outgoing part of the wave instead of the incoming one. Using these auxiliary solutions, one can then form a linear combination that solves the original problem (7) as

$$\psi_{nj} = \sum_{j_0} C_{j_0} \psi_{nj}^{(j_0)}. \tag{17}$$

The coefficients $A_j^{j_0}$ in Eqs. (15) and (16) are determined such that (14) can be solved as discussed in Appendix A. Demanding that the linear combination (17) satisfies the original boundary conditions Eqs. (9) and (10), we obtain the following system of equations for the coefficients $C_{j_0}$:

$$\sum_{j_0} A_j^{j_0} C_{j_0} = \delta_{jj_{\text{in}}}. \tag{18}$$

Since the matrix $[A_j^{j_0}]$ is always regular, we can find its inverse $Q_{j_0}^j$ and then the coefficients $C_{j_0} = Q_{j_0}^{j_{in}}$ of the expansion (17). After $C_{j_0}$'s are determined, the reflection and transmission amplitudes $\mathfrak{R}_j(k_{in})$ and $\mathfrak{T}_j(k_{in})$ simply follow from:

$$\mathfrak{T}_j(k_{in}) = C_j, \tag{19a}$$

$$\mathfrak{R}_j(k_{in}) = \sum_{j_0} \left( \delta_{j j_0} - A_j^{j_0} \right) C_{j_0}. \tag{19b}$$

The main advantage of this method over directly solving the eigenvalue problem Eq. (7) with the boundary conditions Eqs. (9) and (10) is that the choice of the boundary conditions Eq. (16) eases the burden of obtaining the probability amplitude on the scatterers, which are essential to solve the problem (Appendix A).

The method can be implemented for any configuration of the scatterer without any restrictions on the number of monomers in the scatterer. It can even be modified for cases in which the scatterer interacts with several monomers of the main chain. The contribution to the transmission profile from each channel can be explicitly obtained, and an estimate of the final quantum state of the scatterer can also be deduced.

Next, we apply our QSM approach to the transport system with a CU containing an active vibrational degree of freedom.

## IV. EXCITATION TRANSPORT

### A. Static monomers

Excitation transport in a linear chain of monomers interacting with a static CU, i.e., in the absence of any vibrations, was explored in the past using a TMM to obtain the transmission and reflection coefficients [19], see also Appendix D. Transport was found to be highly sensitive to the resonance properties of the CU, which acts as a defect [16]. Due to the interference between the continuum energies of the main chain and the discrete energies of the control unit, the system exhibits Fano resonances.

We consider the configuration where the CU monomers form a static equilateral triangle, corresponding to angles $\vartheta = [0, 2\pi/3, 4\pi/3]^T$ with a twofold goal: First, to illustrate the features above, and second to benchmark the QSM formulated in Sec. III by comparison with the TMM and with solutions of the TDSE. It was shown in Refs. [19,54,55] that for an incoming energy $E$ the transmission amplitude is

$$T(E) = \frac{4J^2 - E^2}{4J^2 - E^2 + V_{eff}(E)^2}, \tag{25a}$$

$$V_{eff}(E) = \frac{D_2}{D_3} G^2, \tag{20b}$$

with the energy-dependent effective scattering potential $V_{eff}(E)$ from the CU. The latter is determined in the chosen configuration through $D_i = \det(E\mathbb{1} - H_i)$, where $H_3$ and $H_2$ are the dipole-dipole Hamiltonian of the CU and of the CU without the entrance site $\alpha$, respectively, as derived in Appendix D. One sees from (20), that transmission is completely suppressed if $V_{eff}$ tends to infinity, which happens if $D_3 = 0$, i.e., whenever the energy $E$ coincides with an eigenenergy of $H_3$. On the other hand, if the energy $E$ matches an eigenenergy
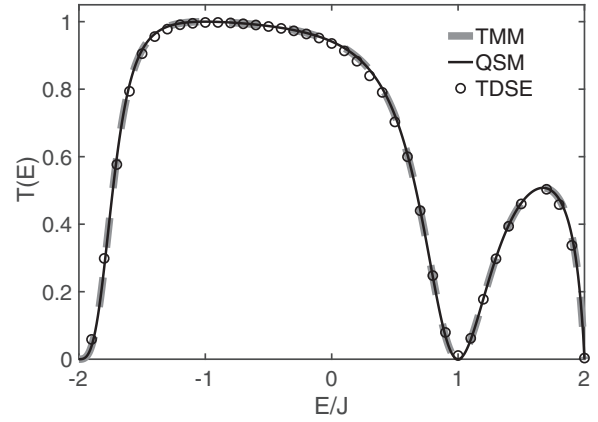


FIG. 3. Total transmission through the chain as a function of energy for fixed monomers, and the control unit forming an equilateral triangle with further parameters given in Ref. [50]. Results obtained with the quantum scattering method (QSM) (thin solid line) with a time-dependent wave-packet propagation (○) and the transfer matrix method (TMM) (thick dashed line) are shown.

of $H_2$ we have $D_2 = 0$ implying that $V_{eff} = 0$, and, therefore, the transmission is maximal $T = 1$. Furthermore, for any finite value of $V_{eff}$, transmission is fully suppressed at $E = \pm 2J$.

These properties can be directly found in the transmission profile shown in Fig. 3. First, one can appreciate that results from the TMM and calculated with the more complex QSM formalism in Sec. III as well as TDSE solutions agree well. The CU $\hat{H}_U = H_3$ has two degenerate eigenenergies at $E = J$ and a third one at $E = -2J$ since we choose $F = F_{\alpha\beta} = F_{\alpha\eta} = F_{\beta\eta} = J$. In contrast the reduced control unit without the entrance site $\hat{H}'_U = H_2$ has two eigenenergies $E_\pm = \pm J$. Hence, we expect transmission extrema at $E = \pm 2J$ and $E = \pm J$, more precisely zero transmission at energies $\pm 2J$ and $J$ and full transmission at $E = -J$, which is in accordance with Fig. 3. The complete suppression of transport at $J = 1$ has an asymmetric profile, characteristic for a Fano resonance. Its width depends on the interaction strength between the main chain and the CU determined by the relative position of the CU with respect to the chain. It is clearly sensitive to details of the CU since $E = J$ is an eigenenergy for both, $H_2$ and $H_3$. However, the influence of the latter dominates as its eigenstate is doubly degenerate.

The QSM has been developed to study the transport properties for the vibrating CU with a motional degree of freedom. To compare it with the static CU case discussed in this section, we only allow the ground-state $j = 0$ in all sums of Sec. III, effectively freezing the motional degree of freedom. We also call this scenario "immobile." As can be seen in Fig. 3, the immobile QSM is equivalent to a static calculation using the TMM. The QSM for an immobile CU, and the TMMs require comparable computational effort. Although the TMM takes into account an effective scattering potential, QSM exactly determines the state of the scatterer and provides the transmission and reflection coefficients through proper boundary conditions in the Schrödinger equation.

For final verification, we also solve the TDSE with the complete Hamiltonian (3a). To obtain the transmission profile, we take the Gaussian wave packet of electronic states
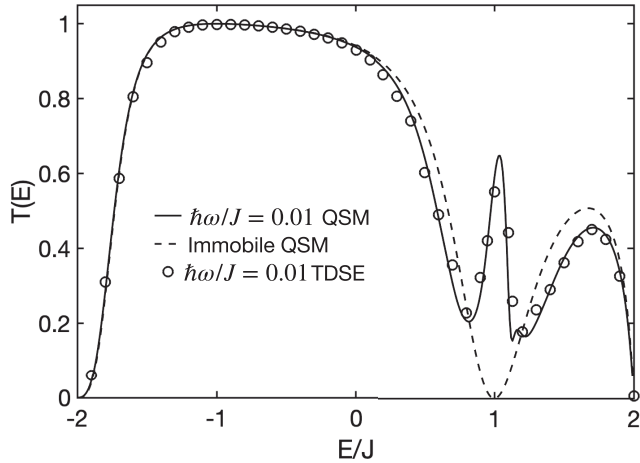
FIG. 4. Comparison of transmission profile for vibrating and immobile monomer $\alpha$ in the control unit. The dashed curve shows the transmission profile obtained from our multichannel quantum scattering method (QSM) when the vibrational state is constrained to the ground state. The solid curve shows the transmission profile obtained from the QSM for the vibrating monomer with harmonic frequency $\hbar\omega/J = 0.01$ and other parameters as in Ref. [50]. Circles show the transmission profile obtained from a time-dependent wave-packet calculation for verification. For the QSM, here and elsewhere, we use 50 vibrational states unless otherwise indicated with results unchanged for higher numbers. Here and in the subsequent plots, monomer $\alpha$ is assumed to be initially in the vibrational ground-state $j_{\mathrm{in}} = 0$.

$|\psi_{\mathrm{ini}}\rangle$ introduced in Sec. II B on the far left of the linear chain as the initial condition for the incoming excitation. The integrated transmitted probability after the excitation has left the scattering region provides the transmission coefficient. These numerical solutions are obtained using XMDS [56,57]. We see in Fig. 3 that the transmission coefficient obtained from the TDSE matches well with the QSM and TMM results with minor deviations caused by the finite energy width of the Gaussian wave packet. This enables us to use the TDSE solutions to verify the results obtained from the QSM also in the case of vibrations in the CU, which is our final goal and discussed in the next section.

### B. Fano resonances with vibrations

To see how electronic-vibrational coupling affects the quantum transport, we now mobilize monomer $\alpha$ of the CU such that it can execute small harmonic vibrations with frequency $\omega$ on the circle around its equilibrium position. Since $\hbar\omega \sim J$, several vibrational levels with energy $\hbar\omega(j + 1/2)$ can be excited from the vibrational ground-state $j_{\mathrm{in}} = 0$ by the incoming electronic wave packet with energies of the exciton band in the range of $[-2J, 2J]$. Constraining all but one monomer is for simplicity only, our methods can be generalized to include vibrations of all control unit monomers.

In Fig. 4, we compare the transmission profile obtained from the QSM for the immobile and mobile scatterer. Allowing vibrations (here with a small frequency $\hbar\omega = 0.01J$) clearly modifies the Fano profile most significantly close to the Fano resonance dip at $E = J$ where we see finite trans-

mission instead of full reflection in the immobile case. In contrast, vibrations leave the other regions of the transmission spectrum largely unaffected. In particular, the perfect transmission at $E = -J$ and reflection at $E = \pm 2J$ persist. This may be understood realizing that these characteristics are due to the reduced CU $\hat{H}'_U$ and the chain just in the presence of a CU, respectively. The conditions for both of these elements remain the same if $\alpha$ is mobilized. For the dramatic change in transmission, the dynamic character of vibrations must be included. For example, one cannot average the static TMM results of Sec. IV A over some extended spatial distribution of monomer $\alpha$ (see Appendix E).

Empirically, a CU with three sites is the minimal configuration to easily achieve the desired large influence of vibrations, i.e., significant broadband transmission in the presence of vibrations for incoming energies that are opaque in the static case. This can be understood through the fragility of the quotient $D_2/D_3$ in the static case Eq. (20), for the case where numerator and denominator both tend to zero. This control unit, thus, gives rise to a *qualitative impact* of vibrations on transport. Strictly speaking, a single vibrating monomer in the control unit is sufficient to influence transport on the chain, although to a much smaller extent and only for a very narrow regime of parameters which required excessive parameter tuning to find. Moreover, for a single monomer in the CU, both the coupling between CU and main chain as well as the coupling strength to higher vibrational excitations depend on a single physical parameter the interaction strength between the CU and the main chain. For more monomers in the CU, the coupling strength to higher vibrational excitations additionally depends on intra-CU interactions, allowing the two crucial quantities to be independently tuned.

For verification of the QSM results, we compare them to those obtained with the TDSE. In contrast to the previous section, we explicitly include the vibrational dynamics of monomer $\alpha$ in the simulation, which is initialized in the vibrational ground state. After the scattering event, the transmission coefficient shown in Fig. 4 is obtained as discussed before, summing over all vibrational channels. The TDSE quantitatively confirms the transmission profile, in particular, the spectacular switch of the suppression around $E = J$ to a local maximum of transmission due to an excitable CU.

### 1. Distinguishing vibrational channels

The QSM allows us to separately quantify the contribution of each vibrational channel $j$ as performed in Fig. 5 where the individual transmission probabilities $T_j$ are shown together with the total transmission $T = \sum_j T_j$. Partial transmission $T_j$ means that the vibrating monomer remains in vibrational state $|j\rangle$ *after* the excitation has passed the control unit region and, hence, can no longer affect the vibrational state. One sees from Fig. 5(a) that the elastic channel without lasting energy exchange between main chain and CU dominates transmission apart from energies close to the resonance at $E = J$. This remains true even if the initial vibrational state for the monomer is not the ground state as in Fig. 5 but rather an excited state. We see that only even $j$ contribute here due to the mirror symmetry of the setup in Fig. 1. Without this symmetry also odd $j$ would contribute.
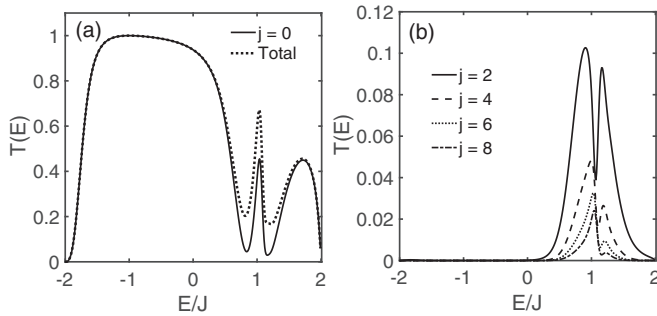
FIG. 5. Contributions of different vibrational channels: (a) Total transmission profile (dotted line), compared to the elastic channel, i.e., for $j_{in} = j_{final} = 0$ (solid line). (b) Contribution from inelastic channels with $j_{final} > 0$. The harmonic frequency for monomer $\alpha$ is $\hbar\omega/J = 0.01$ and other parameters as in Ref. [50].

The transmission profile associated with the $|j_{in}\rangle$ channel is similar to the static case except in the vicinity of $E = J$ where a nonzero transmission is observed. Other channels contribute quite significantly to transmission in the dip region where a small finite transmission contribution is found, which decreases with the inelasticity, i.e., with increasing vibrational energy of the channel, see Fig. 5(b). The sum of total transmission and reflection over all channels is unity for the entire energy region, confirming the consistency of the method.

#### 2. Vibrational resonances

So far we have focused on small vibrational frequencies $\hbar\omega \ll J$. High vibrational frequencies $\hbar\omega > 2J$ lead to quantized vibrational states outside the exciton band which are weakly coupled for our parameters. The transmission profile for the excitation transport is shown in Fig. 6 for several vibrational frequencies $\omega$. As expected, if $E = J + \hbar\omega$ falls outside the exciton bandwidth, here for $\hbar\omega \geqslant J$, the transmission profile is not affected by the vibration, see thick gray curve in Fig. 6(a). For lower frequencies a clear feature appears at $E = J + \hbar\omega$, in the form of a narrow peak and dip, superimposing the already existing broad dip centered at $E = J$. The characteristic profile seen again heralds a Fano resonance that now involves the vibration of the monomer in addition to electronic degrees of freedom. As $\omega$ is further reduced,
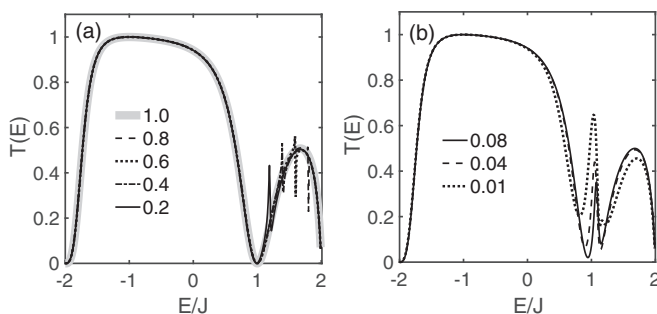


FIG. 6. Transmission as a function of energy for different vibration frequencies of the ring monomer with parameters given in Ref. [50]. The legends indicate the vibrational energy $\hbar\omega/J$. (a) Frequencies $\hbar\omega \geqslant 0.2$. (b) Frequencies $\hbar\omega/J < 0.2$.
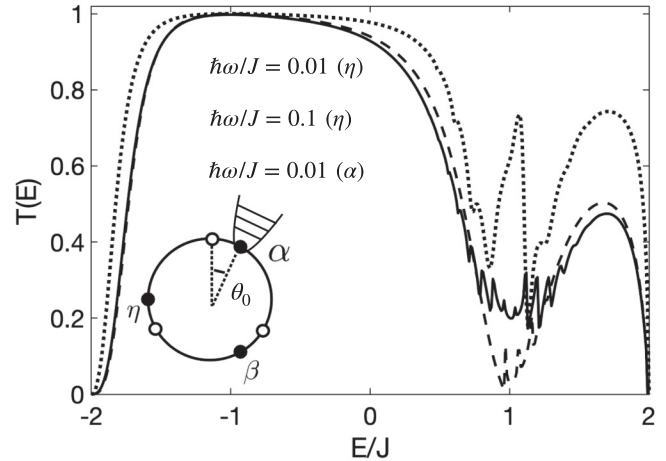


FIG. 7. Transmission as a function of energy for two harmonic frequencies $\omega_\eta$ of the ring monomer $\eta$ with parameters given in Ref. [50] and the two other monomers of the CU kept immobile. Transmission spectrum (dotted) for an asymmetric CU configuration where only monomer $\alpha$ is mobile, and the CU has been rotated by $\theta_0 = \pi/6$ (see the inset) relative to the main chain.

the resonance peaks move towards $E = J$ and broaden giving rise to transmission instead of reflection at $J = 1$ as discussed before, see Fig. 4(b).

#### 3. More vibrations and transmission switching

Although we have only considered vibrations on monomer $\alpha$ so far, let us briefly inspect what happens if monomer $\eta$ is mobile instead ($\eta$ and $\beta$ are equivalent by symmetry). For $\hbar\omega_\eta/J \geqslant 0.1$ (dashed line in Fig. 7) the transmission profile is qualitatively similar to the case of a static CU, whereas multiple resonance kinks appear for the smaller frequency $\hbar\omega/J = 0.01$ (solid line in Fig. 7) turning the transmission dip into a region of finite transmission.

Note that monomers $\alpha$ and $\eta$ play a very different role for our transport system which is most easily seen in the static case from our discussion of Eq. (20) where the eigenenergies of the CU with $\alpha$, $D_3$, and the eigenergies of the reduced CU $H_2$ (including $\eta$ but excluding $\alpha$) enter the effective potential $V_{eff}$ as a factor of $D_2/D_3$. The difference of the roles can be blurred with an asymmetric CU configuration which is achieved by simply rotating the entire CU with an angle $\theta_0$ as shown in the inset of Fig. 7. Indeed, now the transmission for a mobile monomer $\alpha$ keeping the other two monomers in the CU immobile, shows additional resonance features similar to a mobile $\eta$ before, whereas retaining the overall characteristics of mobile $\alpha$ from the symmetric case with a sizable transmission at $E = J$, see dotted line in Fig. 7.

Importantly, in either case, with vibrations on $\eta$ or $\alpha$, we find that a spectral region of perfect reflection can be turned into one with significant finite transmission. This signals a complete qualitative change of resonant scattering through motion of the CU monomers. A general understanding of this behavior is provided by nonadiabatic transitions between chain states discussed in Ref. [58] within an appropriate time-dependent framework.

The QSM presented here provides a clear picture of electronic transmission in the presence of few vibrations but can also provide a computational tool for the inclusion of a large number $N_{\mathrm{modes}}$ of vibrational modes. For that purpose, the computational effort scales cubic with the total number of vibrational states and, thus, exponential with the number of modes $N_{\mathrm{modes}}$ as is commonly the case.

## V. CONCLUSIONS AND OUTLOOK

To describe the effect of vibrating sites in discrete transport systems we have developed a multichannel quantum scattering method (QSM) which allows us to determine transmission and reflection coefficients in a time-independent framework, despite the strong coupling of excitation transport to vibration and creation of electronic-vibrational entanglement. We have verified the results and the QSM developed, by extensive comparison with time-dependent wave-packet calculations using the TDSE. Since a larger number of vibrating sites can be included, the method is applicable in a general context of transport on a discrete chain of sites with coupling to vibration or intersite motion, ranging from conjugated polymers and molecular wires and coupled quantum dots with involvement of phonons to optomechanical arrays.

Using this method, we have explored how Fano resonances in quantum transmission on a static chain of discrete sites (monomers) including a control unit (scatterer) are modified if the monomers are allowed to vibrate. This setup constitutes a Fano-Anderson chain with mobile scatterers. It gives rise to rich features, including the reversal of the scattering effect: Mobile scatterers can lead to significant transmission at incoming wave energies with full reflection in the static case. The qualitative difference of the transmission characteristics close to a Fano resonance with significant transmission upon different kinds of monomer mobilization in the control unit suggests possible applications in nanoscopic switching and sensing.

## ACKNOWLEDGMENTS

## APPENDIX A: VIBRATIONAL CHANNEL EXPANSION COEFFICIENTS

Here, we describe the steps to obtain the coefficients $A_j^{j_0}$ in Eqs. (15) and (16). To solve the eigenvalue problem (14), let us first look at the action of the Hamiltonian $\hat{H}$ on state $|\Psi\rangle$

defined in Eq. (8). Noting that $\langle nj|\Psi\rangle = \psi_{nj}$, we find

$$
\begin{aligned}
&\langle nj|\hat{H}|\Psi\rangle \\
&= [1 - (\delta_{n\alpha} + \delta_{n\beta} + \delta_{n\eta})][J\psi_{n+1,j} + J\psi_{n-1,j}] + \mathcal{E}_j\psi_{nj} \\
&\quad + (\delta_{n\alpha} + \delta_{n\beta} + \delta_{n\eta}) \sum_{n' \in (\alpha,\beta,\eta)}^{n' \neq n} \sum_{j'} F_{nn'}^{jj'} \psi_{n'j'} \\
&\quad + \delta_{n0} \sum_{j'} G^{jj'} \psi_{\alpha j'} + \delta_{n\alpha} \sum_{j'} G^{jj'} \psi_{0j'}.
\end{aligned} \tag{A1}
$$

The terms $\sim J, \mathcal{E}_j$ on the right pertain to the main chain, the term $\sim F$ to the control unit, and the terms $\sim G$ represent the coupling between main chain and the control unit. The coefficients $F$ and $G$ are matrix elements of the electronic-vibrational coupling, given in Eqs. (3e) and (3f), respectively. Details on the calculation of these matrix elements for one exemplary interaction are provided in Appendix B.

In the following we employ the method of backward propagation. Instead of specifying the vibrational state when the excitation is *incoming* as in the problem we intend to solve, we consider the problem where the *outgoing* wave can be assigned a well-defined vibrational quantum number $j_0$. This leads to a simple outgoing boundary condition in (16). This, in turn, implies a more complicated superposition of vibrational states in the incoming and reflected part of the wave function in (15). We can finally assemble a solution that exhibits a specific incoming vibrational state as the linear combination (17) of these auxiliary scattering solutions.

One crucial part of solving the eigenvalue problem is obtaining the probability amplitude on the scatterer. With the regular boundary conditions, this is a difficult task in the presence of many vibrational levels. Below we illustrate the method to find the probability amplitudes on the scatterer, which is essential in solving the auxiliary equations. The particular choice of boundary conditions discussed above along with the auxiliary equations makes this easier.

We can explicitly solve the auxiliary eigenproblem (14) for all the possible values of the index $j_0$. From Eq. (15), we know that $\psi_{0j}^{(j_0)} = \delta_{jj_0}$. This is the key property of the auxiliary problem that simplifies the determination of all vibrational amplitudes in the scatterer compared to the original problem where, in general, all $\psi_{0j}$'s may be nonzero. In order to obtain the wave function associated with the ring, i.e., to get the quantities $\psi_{\bullet j}^{(j_0)} \equiv \{\psi_{\alpha j}^{(j_0)}, \psi_{\beta j}^{(j_0)}, \psi_{\eta j}^{(j_0)}\}$, one can now deal with an inhomogeneous system of linear equations, which is directly obtained from Eqs. (14) and (A1) as

$$
(E - \mathcal{E}_j)\psi_{\alpha j} - \sum_{jj'} F_{\alpha\beta}^{jj'} \psi_{\beta j'} - \sum_{j'} F_{\alpha\eta}^{jj'} \psi_{\eta j'} = \sum_{j'} G^{jj'} \psi_{0j'},
$$

$$
(E - \mathcal{E}_j)\psi_{\beta j} - \sum_{j'} F_{\beta\alpha}^{jj'} \psi_{\alpha j'} - \sum_{j'} F_{\beta\eta}^{jj'} \psi_{\eta j'} = 0,
$$

$$
(E - \mathcal{E}_j)\psi_{\eta j} - \sum_{j'} F_{\eta\alpha}^{jj'} \psi_{\alpha j'} - \sum_{j'} F_{\eta\beta}^{jj'} \psi_{\beta j'} = 0. \tag{A2}
$$

Problem [Eq. (A2)] must always possess a unique solution $\psi_{\bullet j}^{(j_0)}$ as long as the entire theoretical formulation is consistent. After determining the quantities $\psi_{\bullet j}^{(j_0)}$, which depend on all the

$\psi_{0,j'}$'s, the amplitude $\psi_{-1,j}^{(j_0)}$ can be obtained from

$$J\psi_{+1,j} + J\psi_{-1,j} + (\mathcal{E}_j - E)\psi_{0,j} + \sum_{j'} G^{jj'}\psi_{\alpha j'} = 0.$$

It then allows us to find the coefficient $A_j^{j_0}$ after writing down Eq. (15) for the case $n = -1$ and inserting $\psi_{-1,j}^{(j_0)}$ from Eq. (A3). One then finds

$$2iA_j^{j_0} \sin k_j = \delta_{jj_0} e^{+ik_{j_0}} - \psi_{-1,j}. \tag{A3}$$

This completes the explicit solution of the eigenproblem (15).

## APPENDIX B: ELECTRONIC-VIBRATIONAL COUPLING

In this Appendix, we derive the expressions for the components $F_{nn'}^{jj'}$ and $G^{jj'}$ defined in Eqs. (3e) and (3f), respectively, for the specific example of dipole-dipole interactions, where

$$F_{nn'}(\boldsymbol{\vartheta}) = -\frac{\mu^2}{|\mathbf{r}_n(\vartheta_n) - \mathbf{r}_{n'}(\vartheta_{n'})|^3}, \tag{B1}$$

and similarly,

$$G(\boldsymbol{\vartheta}) = -\frac{\mu^2}{|\mathbf{r}_0 - \mathbf{r}_\alpha(\vartheta_\alpha)|^3}, \tag{B2}$$

with transition dipole moment $\mu$ and $\mathbf{r}_n(\vartheta_n)$ as the position of monomer $n$. Other exponents for the distance dependence, such as $1/r^m$ (with $m > 2$) would lead to a structurally similar expression for the matrix elements and, hence, qualitatively similar results. The same would be true for any other interactions for which the interaction between the monomers in the control unit as well as that between main chain and the control unit depends on the distance between the monomers.

Let $\vartheta_{n0}$ denote the central angle of monomer $n$ on the ring where the vibrational potential has its minimum. The angular position of monomer $n$ is given by $\vartheta_n$, and the displacement, hence, defined as $\Delta_n$ as $\vartheta_n - \vartheta_{n0}$. The trap potential in the position representation is then,

$$V_{\text{trap}}(\Delta_n) = \tfrac{1}{2} M\omega^2 R^2 [2(1 - \cos \Delta_n)] \tag{B3}$$

$$\approx \tfrac{1}{2} M\omega^2 (R\Delta_n)^2. \tag{B4}$$

### 1. Calculation of $F_{nn'}^{jj'}$

We now focus in the term $F_{nn'}$, i.e., interaction between monomers on the ring. The inverse cubed distance between two monomers $n$ and $n'$ on the ring can be expressed through their angular coordinates $\vartheta_n$ and $\vartheta_{n'}$ as

$$r_{nn'}^{-3} = \frac{2^{-3/2}}{R^3} [1 - \cos (\vartheta_n - \vartheta_{n'})]^{-3/2}. \tag{B5}$$

The angular separation between monomers $n$ and $n'$ is denoted by $\vartheta_{nn'} = \vartheta_n - \vartheta_{n'}$, hence, an equidistant configuration of them corresponds to $|\vartheta_{nn'}| = 2\pi/3$ for all pairs $n, n'$. For convenience let $\Delta_{nn'} = \Delta_n - \Delta_{n'}$. We then can write

$$r_{nn'}^{-3} = \frac{2^{-3/2}}{R^3} [1 - \cos(\vartheta_{nn'} + \Delta_{nn'})]^{-3/2}. \tag{B6}$$

Assuming the displacements to be small, a Taylor expansion of the function $f(\Delta_{nn'}) = [1 - \cos(\vartheta_{nn'} + \Delta_{nn'})]^{-3/2}$ up to first order around $\Delta_{nn'} = 0$ gives

$$f(0) = (1 - \cos \vartheta_{nn'})^{-3/2} \equiv F_0^{nn'}, \tag{B7}$$

$$f'(0) = -\tfrac{3}{2}(1 - \cos \vartheta_{nn'})^{-5/2} \sin \vartheta_{nn'} \equiv F_1^{nn'}. \tag{B8}$$

Hence the approximate inverse cubed distance is

$$r_{nn'}^{-3} = \frac{2^{-3/2}}{R^3}\left(F_0^{nn'} + F_1^{nn'} \Delta_{nn'}\right). \tag{B9}$$

This leads to

$$F_{nn'}^{jj'} = {}_{\text{vib}}\langle \Phi_j | F_{nn'}(\boldsymbol{\vartheta}) | \Phi_{j'} \rangle_{\text{vib}}$$

$$= \delta_{j_z j_z'} \iint d(R\Delta_n) d(R\Delta_{n'}) \Phi_{j_x}(R\Delta_n) \Phi_{j_y}(R\Delta_{n'})$$

$$\times (F_0^{nn'} + F_1^{nn'} \Delta_{nn'}) \Phi_{j_x'}(R\Delta_n) \Phi_{j_y'}(R\Delta_{n'}). \tag{B10}$$

Here $z$ denotes the monomer index on the ring that should be neither $n$ nor $n'$, which is uniquely determined since for this term we also require $n \neq n'$ and there are only three monomers in total. $j \equiv \{j_\alpha, j_\beta, j_\eta\}$ represents the vibrational state of each monomer in ring and $x, y, z \in \{\alpha, \beta, \eta\} \backslash \{n, n'\}$. For example, if $n = \alpha$ and $n' = \eta$, then $j_\alpha \to j_x$, $j_\beta \to j_z$, and $j_\eta \to j_y$ and, hence, $j$ and $j'$ can be written as $j \equiv \{j_x, j_z, j_y\}$ and $j' \equiv \{j_x', j_z', j_y'\}$. Furthermore, the complex conjugation of the eigenfunctions is omitted since those are real. Finally, since a finite number of modes are included, the integration can be formally extended from $-\infty$ to $+\infty$. Hence,

$$F_{nn'}^{jj'} = \delta_{j_z j_z'}(I_0 + I_1), \tag{B11}$$

where

$$I_0 = F_0^{nn'} \delta_{j_x j_x'} \delta_{j_y j_y'}, \tag{B12}$$

$$I_1 = F_1^{nn'} \iint d(R\Delta_n) d(R\Delta_{n'}) \Phi_{j_x}(R\Delta_n) \Phi_{j_y}(R\Delta_{n'})$$

$$\times (\Delta_n - \Delta_{n'}) \Phi_{j_x'}(R\Delta_n) \Phi_{j_y'}(R\Delta_{n'}) \tag{B13}$$

$$= F_1^{nn'} \int d(R\Delta_n) \Phi_{j_x}(R\Delta_n) \Delta_n \Phi_{j_x'}(R\Delta_n)$$

$$- \int d(R\Delta_{n'}) \Phi_{j_y}(R\Delta_{n'}) \Delta_{n'} \Phi_{j_y'}(R\Delta_{n'}). \tag{B14}$$

Using the explicit form of the eigenfunction in terms of Hermite polynomials $H_j(x)$, the first integral in Eq. (B14) becomes

$$\int d(R\Delta_n) \Phi_{j_x}(R\Delta_n) \Delta_n \Phi_{j_x'}(R\Delta_n)$$

$$= \sqrt{\frac{M\omega}{\pi\hbar}} \frac{1}{\sqrt{2^{j_x+j_x'} j_x! j_x'!}} \int d(R\Delta_n) H_{j_x}\left(\sqrt{\frac{M\omega}{\hbar}} R\Delta_n\right)$$

$$\times \Delta_n H_{j_x'}\left(\sqrt{\frac{M\omega}{\hbar}} R\Delta_n\right) \exp\left(-\frac{M\omega}{\hbar} R^2 \Delta_n^2\right) \tag{B15}$$

$$= \frac{1}{2R} \sqrt{\frac{\hbar}{\pi M\omega}} \frac{1}{\sqrt{2^{j_x+j_x'} j_x! j_x'!}}$$

$$\times \int dX \, H_{j_x}(X) H_{j_x'}(X) H_1(X) \exp(-X^2), \tag{B16}$$

where $X = \sqrt{\frac{M\omega}{\hbar}} R\Delta_n$ and $X = H_1(X)/2$.

This integral vanishes whenever $j_x + j'_x + 1$ is odd since in this case the integrand is odd and the integration interval symmetric. Moreover, one needs $|j_x - j'_x| = 1$ since after Taylor expansion to first order the harmonic-oscillator ladder operators couple only adjacent vibrational states. For even $j_x + j'_x + 1$ we can obtain [59]

$$\int dX \, H_{j_x}(X) H_{j'_x}(X) H_1(X) \exp(-X^2)$$
$$= \frac{2^{s_x} \sqrt{\pi} \, j_x! j'_x!}{(s_x - j_x)!(s_x - j'_x)!(s_x - 1)!}, \qquad \text{(B17)}$$

with $s_x = \frac{j_x + j'_x + 1}{2}$. Since $|j_x - j'_x| = 1$, $(s_x - j_x)!(s_x - j'_x)!(s_x - 1)! = (\frac{j_x + j'_x - 1}{2})!$. Now let

$$\Gamma(v, w) = \frac{\sqrt{v! w!}}{(\frac{v + w - 1}{2})!}. \qquad \text{(B18)}$$

Then $I_1$ can be written as

$$I_1 = F_1^{nn'} \frac{1}{R} \sqrt{\frac{\hbar}{2M\omega}} [\Gamma(j_x, j'_x) - \Gamma(j_y, j'_y)]. \qquad \text{(B19)}$$

Thus,

$$F_{nn'}^{jj'} = -\frac{\mu^2}{(\sqrt{2}R)^3} \delta_{j_z j'_z} \left( F_0^{nn'} \delta_{j_x j'_x} \delta_{j_y j'_y} \right.$$
$$\left. + \frac{F_1^{nn'}}{R} \sqrt{\frac{\hbar}{2M\omega}} [\Gamma(j_x, j'_x) - \Gamma(j_y, j'_y)] \right), \qquad \text{(B20)}$$

with $F_k^{nn'}$ defined in Eqs. (B7) and (B8). Finally, since $|j_x - j'_x| = 1$ and $|j_y - j'_y| = 1$, we can write

$$\Gamma(j_x, j'_x) - \Gamma(j_y, j'_y) = \sqrt{j_x + 1} \delta_{j'_x, j_x+1} + \sqrt{j'_x + 1} \delta_{j'_x+1, j_x}$$
$$- \sqrt{j_y + 1} \delta_{j'_y, j_y+1} - \sqrt{j'_y + 1} \delta_{j'_y+1, j_y}. \qquad \text{(B21)}$$

### 2. Calculation of $G^{jj'}$

Now consider the matrix elements of $\hat{H}_{SC}$. The position of the trap $\alpha$ is at $0°$, and so the inverse cubed distance can, for small $\Delta_\alpha$, be approximated by

$$r_{\alpha,0}^{-3} \approx [(d - R)^3 + R^2 \sin^2 \Delta_\alpha]^{-3/2}. \qquad \text{(B22)}$$

However, in the Taylor expansion of the right-hand side around $\Delta_\alpha = 0$, the first nonvanishing term beyond the zeroth order is $\sim \Delta_\alpha^2$ so that one may as well directly approximate $r^{-3} \approx (d - R)^{-3}$. This leads to

$$G^{jj'} = -\frac{\mu^2}{(d - R)^3} \delta_{jj'} \delta_{0,\alpha}. \qquad \text{(B23)}$$

### APPENDIX C: TDSE

The quantum dynamics of the system is governed by the time-dependent Schrödinger equation,

$$i\hbar \frac{d}{dt} |\psi(t)\rangle = \hat{H} |\psi(t)\rangle, \qquad \text{(C1)}$$

where $\hat{H}$ is the full Hamiltonian of the system. Explicitly writing the equation for the state (5), we get

$$i\hbar \dot{\psi}_{nj} = [1 - (\delta_{n\alpha} + \delta_{n\beta} + \delta_{n\eta})](J\psi_{n+1,j}$$
$$+ J\psi_{n-1,j}) + \mathcal{E}_j \psi_{nj}$$
$$+ (\delta_{n\alpha} + \delta_{n\beta} + \delta_{n\eta}) \sum_{n' \in (\alpha,\beta,\eta)}^{n' \neq n} \sum_{j'} F_{nn'}^{jj'} \psi_{n'j'}$$
$$+ \delta_{n0} \sum_{j'} G^{jj'} \psi_{\alpha j'} + \delta_{n\alpha} \sum_{j'} G^{jj'} \psi_{0j'}. \qquad \text{(C2)}$$

A Gaussian wave packet far left of the side unit, representing the incoming excitation, is our initial condition for solving Eq. (C1). Initially, the monomers on the circle are assumed to be in the vibrational ground state. The excitation propagates freely towards the right as long as the $n = 0$ site remains unpopulated. During this precollision time interval, vibrational degrees of freedom of the ring monomers are unaffected by the incoming excitation and, hence, remain in the original stationary state. The dynamical time evolution remains governed solely by the first term ($\hat{H}_S$) in the Hamiltonian. The situation changes significantly as soon as the excitation reaches the $n = 0$ site. The other terms in the Hamiltonian become important, and a complicated vibrational quantum dynamics takes place until the excitation completely leaves the scattering region. The electronic-vibrational coupling term in the Hamiltonian could take the monomer to the higher vibrational states and thereby influence the excitation transport in the main chain. The postcollision dynamics is again essentially governed by $\hat{H}_S$.

The excitation probability of the monomers on the left or the right of the Fano defect obtained during the precollision and postcollision period can be used to define a transmission and reflection coefficient. In addition, the contribution from each channel to the transmission coefficient can also be calculated from the dynamics by projecting the spatial wave function onto harmonic-oscillator states after the scattering.

A Gaussian wave packet has an energy width arising from spatial localization within $\Delta$ given by

$$\Delta E_{\text{packet}} \approx \frac{2\hbar^2 k}{m\Delta}, \qquad \text{(C3)}$$

where the mass $m$ in a tight-binding contest can be expressed as $m = \frac{1}{\frac{1}{\hbar^2} \frac{d^2 E}{dk^2}}$ and $k$ is the wave vector.

### APPENDIX D: TRANSFER-MATRIX METHOD

In this Appendix we consider the arrangement of Fig. 1 for static sites. With the full state $|\Psi\rangle = \sum_n \psi_n |n\rangle$ the time-independent Schrödinger equation for quantum scattering of incoming waves on the CU turns into

$$E\psi_n = J\psi_{n+1} + J\psi_{n-1} + G\psi_\alpha \delta_{n,0},$$
$$E\psi_\alpha = F_{\alpha\beta}\psi_\beta + F_{\alpha\eta}\psi_\eta + G\psi_0,$$
$$E\psi_\beta = F_{\beta\alpha}\psi_\alpha + F_{\beta\eta}\psi_\eta,$$
$$E\psi_\eta = F_{\eta\alpha}\psi_\alpha + F_{\eta\beta}\psi_\beta, \qquad \text{(D1)}$$

where we have used the shorthand notation $G = G^{00}$ with $G^{ij'}$ defined in (3f). Rearranging (D2) gives

$$E\psi_n = J\psi_{n+1} + J\psi_{n-1} + \frac{D_2}{D_3}G^2\psi_0\delta_{n,0} \qquad \text{(D2)}$$

with $D_2 = \det(E\mathbb{1} - H_2)$, $D_3 = \det(E\mathbb{1} - H_3)$, where

$$H_3 = \begin{bmatrix} 0 & F_{\alpha\beta} & F_{\alpha\eta} \\ F_{\beta\alpha} & 0 & F_{\beta\eta} \\ F_{\eta\alpha} & F_{\eta\beta} & 0 \end{bmatrix}, \quad H_2 = \begin{bmatrix} 0 & F_{\beta\eta} \\ F_{\eta\beta} & 0 \end{bmatrix} \qquad \text{(D3)}$$

are the dipole-dipole Hamiltonian of the CU ($H_3$) and of the reduced CU without the entrance site ($H_2$). We see in (D2) that the CU acts, such as a localized defect on site $n = 0$. The strength of the effective defect potential,

$$V_{\text{eff}} = D_2 G^2/D_3 \qquad \text{(D4)}$$

depends on the energy of the incoming excitation through $D_j$. If it matches one of the eigenenergies of the side-unit $D_3 = 0$ and the diverging effective scattering potential leads to a total reflection of the incoming wave. In contrast, when for energies resonant on eigenenergies of the side unit minus the entrance site $D_2 = 0$, the effective scattering potential vanishes, and we have perfect transmission [60].

To explicitly evaluate the reflection and transmission coefficient at other energies, we make the usual ansatz,

$$\psi_n = i_{\text{in}}e^{+ikn} + r_{\text{o}}e^{-ikn}, \quad n < 0, \qquad \text{(D5)}$$

$$\psi_n = t_{\text{o}}e^{+ikn}, \quad n > 0. \qquad \text{(D6)}$$

Equation (D2) can be written in the form

$$\begin{bmatrix} \psi_{n+1} \\ \psi_n \end{bmatrix} = T_n \begin{bmatrix} \psi_n \\ \psi_{n-1} \end{bmatrix}, \qquad \text{(D7)}$$

with a transfer matrix,

$$T_n = \begin{bmatrix} \frac{E}{J} - \frac{V_{\text{eff}}}{J}\delta_{n,0} & -1 \\ 1 & 0 \end{bmatrix}. \qquad \text{(D8)}$$

Thus,

$$\begin{bmatrix} \psi_{n+1} \\ \psi_n \end{bmatrix} = P_n \begin{bmatrix} \psi_{-n} \\ \psi_{-n-1} \end{bmatrix}, \qquad \text{(D9)}$$

with $P_n = T_n T_{n-1} \cdots T_{-n}$. Using the boundary conditions in Eqs, (D5) and (D6), the transmission coefficient $T = |t_{\text{o}}|^2/|i_{\text{in}}|^2$ can be obtained from [Eq. (D9)] as [60]

$$T(E) = \frac{4J^2 - E^2}{4J^2 - E^2 + V_{\text{eff}}^2}. \qquad \text{(D10)}$$

with $V_{\text{eff}}$ given in Eq. (D4).

## APPENDIX E: STATIC TRANSMISSION AVERAGES

When approaching smaller vibrational frequencies $\omega$, the zero-point width $\sigma = \sqrt{\hbar/m/\omega}$ of the vibrating monomer increases. Since we can understand transmission for immobile monomers using the TMM discussed in Appendix D, we can attempt to make contact with those calculation by taking the transmission from the TMM for a fixed angle $\theta$ of the
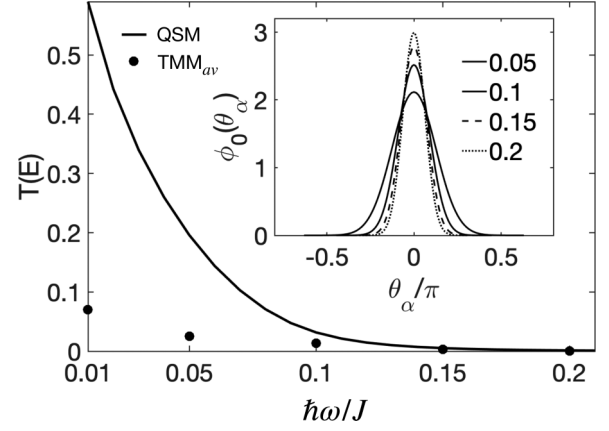


FIG. 8. Transmission as a function of frequency of vibration at the incoming excitation energy $E = J$. The solid line shows the transmission obtained from the QSM. The black dots show the transmission obtained using the static model given by Eq. (E1). The inset: The spacial width of the initial ground state considered for the vibrating monomer $\alpha$ for different vibrational frequencies with energy $\hbar\omega/J$.

vibrating monomer $\alpha$, let that be $T_{\text{TMM}}(\theta)$ and then averaging it according to

$$T = \int T_{\text{TMM}}(\theta)p(\theta)d\theta, \qquad \text{(E1)}$$

over the position distribution $p(\theta)$ in the harmonic-oscillator ground state, shown in the inset of Fig. 8. However, when applied to the scenario of, e.g., Fig. 4 this provides transmission of at most $T \approx 0.08$ near $E = J$, clearly not capturing the essential physics which shows a much more prominent increase of transmission, see Fig. 8. The underlying resonance peak shifts away from $E = J$ as the frequency increases and, thus, the excitation transport increases at lower vibrational frequencies. In contrast, at high frequencies the static picture can give some idea of transmission since motion is suppressed. The transmission as a function of energy $T(E)$ as shown in Fig. 8 differs between the QSM and a static TMM by only 10% at $\hbar\omega = 0.21J$ and 5% at $\hbar\omega = 0.24J$, however, for both cases transmission is strongly suppressed.

## APPENDIX F: PLATFORMS COUPLINGS QUANTUM TRANSPORT AND A FEW VIBRATIONS

We have discussed a single vibrational mode in the main article for clarity, but even this simplified model could be implemented experimentally using a chain of trapped ultra-cold $^7$Li Rydberg atoms. Although, e.g., optical trapping of Rydberg states poses different challenges than for ground-state atoms, it has been demonstrated, in principle [61]. The nearest-neighbor coupling $J = C_3/\delta^3$ for dipole-dipole interaction strength $C_3$ and nearestneighbor separation $\delta$ would be set by dipole-dipole interactions that allow a single Rydberg $p$ ($l = 1$) excitation to migrate on a chain of $s$ ($l = 0$) atoms [62], where $l$ is the angular momentum quantum number. The dipole-dipole interaction strength can be approximated using $C_3 = \mu^2$ and the scaling formula $\mu = \mu_0 \nu^2$ for the transition dipole moment $\mu$, where $\mu_0 = 0.8$ a.u. and $\nu$

is the Rydberg principal quantum number. Similarly, we can estimate the Rydberg state lifetime as $\tau = \tau_0 \nu^3$ with $\tau_0 = 3 \times 10^7$ a.u. [63]. Choosing, e.g., a distance of $\delta = 25\ \mu\text{m}$ and $\nu = 120$ we would have $J = 8.3$ MHz and expect that $N_{\text{hops}} = 150 = \tau/(\pi/J)$ transfers of the excitation from one site to the adjacent one are possible in the lifetime of a chain of $N = 100$ atoms, given by $\tau = \tau_0/N$. This would be sufficient for a realization of the scenario in Fig. 2. Finally, vibrational frequencies of the atom in site $\alpha$ in the range of $0.01 J/\hbar = 83$ kHZ to $J$ used in, e.g., Fig. 6 can be engineered, whereas all other sites can be more tightly trapped to freeze those vibrations.

Although the platform above might provide good control for the experimental verification of our predictions, we envisage the main utility of our method in the study of energy or charge transport in supramolecular structures. One example

is the transport of excitation energy in molecular aggregates [23], another electron transport in molecular wires [64]. Both transport processes are coupled to vibrations of the constituent particles. In the latter setting, exemplary energy scales would be $J = 2.66$ eV [64], then $\hbar\omega$ would be on the order $J/10$ for a $C = C$ stretch vibration. In a generic molecular wire, vibrations would affect all sites equally, however, here a more mobile CU can also be realized by attaching a functional side unit onto a more rigid main wire where the latter could be a double stranded conjugated polymer [65].

Finally, another possible realization of the single vibrational mode model can be in the transport of photons in optomechanical arrays [45,46], which combine the photonic crystal structure in the context of which much of the work in Ref. [19] was developed with localized well-controlled modes of vibration.

[1] A. S. Davydov, Sov. Phys. Usp. **7**, 145 (1964).

[2] H. Haken and P. Reineker, Z. Phys. **249**, 253 (1972).

[3] P. J. Scherer, E. Knapp, and S.-F. Fischer, Chem. Phys. Lett. **106**, 191 (1984).

[4] H. Van Amerongen, R. Van Grondelle *et al.*, *Photosynthetic Excitons* (World Scientific, Singapore, 2000).

[5] O. Kühn and V. Sundström, J. Chem. Phys. **107**, 4154 (1997).

[6] P. Rebentrost, M. Mohseni, I. Kassal, S. Lloyd, and A. Aspuru-Guzik, New J. Phys. **11**, 033003 (2009).

[7] F. Robicheaux, J. V. Hernández, T. Topçu, and L. D. Noordam, Phys. Rev. A **70**, 042703 (2004).

[8] C. Ates, A. Eisfeld, and J.-M. Rost, New J. Phys. **10**, 045030 (2008).

[9] O. Mülken, A. Blumen, T. Amthor, C. Giese, M. Reetz-Lamour, and M. Weidemüller, Phys. Rev. Lett. **99**, 090601 (2007).

[10] S. Wüster, C. Ates, A. Eisfeld, and J.-M. Rost, Phys. Rev. Lett. **105**, 053004 (2010).

[11] D. Barredo, H. Labuhn, S. Ravets, T. Lahaye, A. Browaeys, and C. S. Adams, Phys. Rev. Lett. **114**, 113002 (2015).

[12] G. D. Scholes and G. Rumbles, *Materials For Sustainable Energy: A Collection of Peer-Reviewed Research and Review Articles from Nature Publishing Group* (World Scientific, Singapore, 2011), pp. 12–25.

[13] J. von Neumann and E. P. Wigner, in *The Collected Works of Eugene Paul Wigner*, edited by A. S. Wightman, The Collected Works of Eugene Paul Wigner (Part A: The Scientific Papers. Part B: Historical, Philosophical, and Socio-Political Papers), Vol. A / 1 (Springer, Berlin, Heidelberg, 1993), pp. 291–293.

[14] A. Chakrabarti, Phys. Lett. A **366**, 507 (2007).

[15] P. Singha Deo and C. Basu, Phys. Rev. B **52**, 10685 (1995).

[16] A. E. Miroshnichenko and Y. S. Kivshar, Phys. Rev. E **72**, 056611 (2005).

[17] S. Flach, A. E. Miroshnichenko, V. Fleurov, and M. V. Fistul, Phys. Rev. Lett. **90**, 084101 (2003).

[18] R. A. Vicencio, J. Brand, and S. Flach, Phys. Rev. Lett. **98**, 184102 (2007).

[19] A. E. Miroshnichenko, S. Flach, and Y. S. Kivshar, Rev. Mod. Phys. **82**, 2257 (2010).

[20] A. K. Ismael, I. Grace, and C. J. Lambert, Phys. Chem. Chem. Phys. **19**, 6416 (2017).

[21] A. J. Heeger, Rev. Mod. Phys. **73**, 681 (2001).

[22] A. J. Heeger, S. Kivelson, J. Schrieffer, and W.-P. Su, Rev. Mod. Phys. **60**, 781 (1988).

[23] S. K. Saikin, A. Eisfeld, S. Valleau, and A. Aspuru-Guzik, Nanophotonics **2**, 21 (2013).

[24] S. Wüster, C. Ates, A. Eisfeld, and J.-M. Rost, New J. Phys. **13**, 073044 (2011).

[25] S. Möbius, S. Wüster, C. Ates, A. Eisfeld, and J.-M. Rost, J. Phys. B: At. Mol. Opt. Phys. **44**, 184011 (2011).

[26] S. Möbius, M. Genkin, S. Wüster, A. Eisfeld, and J. M. Rost, Phys. Rev. A **88**, 012716 (2013).

[27] M. Montgomery and T. Todorov, J. Phys.: Condens. Matter **15**, 8781 (2003).

[28] Y.-C. Chen, M. Zwolak, and M. Di Ventra, Nano Lett. **5**, 621 (2005).

[29] F. Sols, Ann. Phys. (NY) **214**, 386 (1992).

[30] H. Ness and A. J. Fisher, Phys. Rev. Lett. **83**, 452 (1999).

[31] J. L. D'Amato and H. M. Pastawski, Phys. Rev. B **41**, 7411 (1990).

[32] A. Troisi and M. A. Ratner, Phys. Rev. B **72**, 033408 (2005).

[33] J. Jiang, M. Kula, W. Lu, and Y. Luo, Nano Lett. **5**, 1551 (2005).

[34] H. Ness, J. Phys.: Condens. Matter **18**, 6307 (2006).

[35] E. G. Petrov, V. May, and P. Hänggi, Chem. Phys. **296**, 251 (2004).

[36] A. Nitzan, Annu. Rev. Phys. Chem. **52**, 681 (2001).

[37] M. Hliwa and C. Joachim, Phys. Rev. B **65**, 085406 (2002).

[38] R. Kline and M. McGehee, J. Macromol. Sci., Polym. Rev. **46**, 27 (2006).

[39] I. Hwang and G. D. Scholes, Chem. Mater. **23**, 610 (2011).

[40] M. A. Ratner, B. Davis, M. Kemp, V. Mujica, A. Roitberg, and S. Yaliraki, Ann. N. Y. Acad. Sci. **852**, 22 (1998).

[41] J. Lehmann, S. Kohler, V. May, and P. Hänggi, J. Chem. Phys. **121**, 2278 (2004).

[42] D. Citrin, Opt. Lett. **20**, 901 (1995).

[43] Y. Kubota and K. Nobusada, J. Chem. Phys. **134**, 044108 (2011).

[44] F. R. Braakman, P. Barthelemy, C. Reichl, W. Wegscheider, and L. M. Vandersypen, Nat. Nanotechnol. **8**, 432 (2013).

[45] A. H. Safavi-Naeini and O. Painter, Opt. Express **18**, 14926 (2010).

[46] M. Ludwig and F. Marquardt, Phys. Rev. Lett. **111**, 073603 (2013).

[47] N. Ashcroft and N. Mermin, *Solid State Physics* (Saunders College, Philadelphia, 1976).

[48] U. Fano, Il Nuovo Cimento **12**, 154 (1935).

[49] U. Fano, Phys. Rev. **124**, 1866 (1961).

[50] In all calculations, the radius of the circle is $R = 0.5774\delta$, $d = 1.5774\delta$ with distances defined in Fig. 1. In the present paper, $\vartheta_{\beta\alpha} = \vartheta_{\eta\beta} = 2\pi/3$ and monomer on-site energies in the ring are $E_n = 0J$. This configuration makes sure that there are eigenvalues of $\hat{H}_{\text{el}}^S$ within the exciton energy band of the main chain $|E| < 2J$, which is essential for providing a Fano resonance. The mass $M$ is selected such that if $\delta = 1$, $M = 110\,00$ a.u. This mass corresponds to a lithium atom for a concrete example where the chain is assembled with dipole-dipole-interacting ultracold Rydberg alkali atoms.

[51] I. Bengtsson and K. Zyczkowski, *Geometry of Quantum States: An Introduction to Quantum Entanglement* (Cambridge University Press, Cambridge, UK, 2006).

[52] D. Y. Sukhanov and M. Kalashnikova, Acoust. Phys. **60**, 304 (2014).

[53] A. Kuzovova and I. Kuzmenko, *MATEC Web of Conferences* (EDP Sciences, Les Ulis, France, 2018), Vol. 155, p. 01019.

[54] P. Tong, B. Li, and B. Hu, Phys. Rev. B **59**, 8639 (1999).

[55] A. E. Miroshnichenko, S. F. Mingaleev, S. Flach, and Y. S. Kivshar, Phys. Rev. E **71**, 036626 (2005).

[56] G. R. Dennis, J. J. Hope, and M. T. Johnsson, Comput. Phys. Commun. **184**, 201 (2013).

[57] G. R. Dennis, J. J. Hope, and M. T. Johnsson, http://xmds.org/.

[58] A. Ramachandran, A. Eisfeld, S. Wüster, and J.-M. Rost (unpublished).

[59] I. S. Gradshteyn and I. M. Ryzhik, *Table of Integrals, Series, and Products* (Academic, Boston, 2014).

[60] E. Kamenetskii, A. Sadreev, and A. Miroshnichenko, *Fano Resonances in Optics and Microwaves* (Springer, Berlin, 2018).

[61] L. Li, Y. O. Dudin, and A. Kuzmich, Nature (London) **498**, 466 (2013).

[62] S. Wüster and J. M. Rost, J. Phys. B: At., Mol. Opt. Phys. **51**, 032001 (2018).

[63] T. F. Gallagher, *Rydberg Atoms* (Cambridge University Press, Cambridge, UK, 1994).

[64] S. Stafström and M. Hultell, in *Charge and Exciton Transport through Molecular Wires*, edited by F. C. Grozema and L. D. A. Siebbeles (Wiley-VCH, Weinheim, 2011), Chap. 8, pp. 207–236.

[65] F. C. Grozema and L. D. A. Siebbeles, in *Charge and Exciton Transport through Molecular Wires*, edited by F. C. Grozema and L. D. A. Siebbeles (Wiley-VCH, Weinheim, 2011), Chap. 1, pp. 1–11.